Effects of strontium doping on the morphological, structural, and photophysical properties of FASnI(3) perovskite thin films

Adjokatse, Sampson; Kahmann, Simon; Duim, Herman; Loi, Maria Antonietta

Published in:
APL Materials

DOI:
10.1063/1.5087110

APL Materials

Effects of strontium doping on the morphological, structural, and photophysical properties of $FASnI_3$ perovskite thin films

Cite as: APL Mater. **7**, 031116 (2019); https://doi.org/10.1063/1.5087110
Submitted: 28 December 2018 . Accepted: 28 February 2019 . Published Online: 27 March 2019

Sampson Adjokatse, Simon Kahmann, Herman Duim, and Maria Antonietta Loi

Effects of strontium doping on the morphological, structural, and photophysical properties of $FASnI_3$ perovskite thin films

Cite as: APL Mater. 7, 031116 (2019); doi: 10.1063/1.5087110
Submitted: 28 December 2018 • Accepted: 28 February 2019 •
Published Online: 27 March 2019

Sampson Adjokatse, Simon Kahmann, Herman Duim, and Maria Antonietta Loi[a]

AFFILIATIONS

Zernike Institute for Advanced Materials, University of Groningen, Nijenborgh 4, 9747 AG Groningen, The Netherlands

Note: This paper is part of the special topic on Perovskite Semiconductors for Next Generation Optoelectronic Applications.
[a]**Author to whom correspondence should be addressed:** m.a.loi@rug.nl

ABSTRACT

Doping engineering has been an effective technique applied extensively to enrich semiconductors and modulate their fundamental properties for electronic and optoelectronic applications. In this work, we report the influence of strontium (Sr) doping on solution-processed formamidinium tin iodide ($FASnI_3$) perovskite thin films. We show that the addition of the Sr^{2+} dopant to the host perovskite drastically changes the morphology of the material but has no significant effect on the structural phase for doping concentrations lower than 10%. Using photoluminescence spectroscopy, we showed that for doping contents below 15%, the film is heterogeneously doped and strontium predominantly resides at the surface of the film. Above 15% of Sr, the bulk of the material is significantly doped. Our results show that Sr doping into $FASnI_3$ perovskite can be a route for the attainment of new perovskites with interesting physical properties.

Organic-inorganic metal halide perovskite semiconductors have attracted considerable attention in recent years. This is due to the great potential they hold as new optoelectronic materials for devices that could be processed using simple and cheap techniques on large areas and flexible substrates.[1–3] Optoelectronic devices such as solar cells,[4–6] light emitting diodes,[7–9] light emitting field-effect transistors,[10–12] lasers,[13–15] photodetectors,[3,16,17] and x-ray detectors[18,19] have already been demonstrated with outstanding performances.

The most extensively studied halide perovskites are the lead (Pb) and tin (Sn) perovskites. Among them, the more stable and high-performing devices are based on the lead-containing perovskites. Unfortunately, they are toxic and water-soluble. Hence, their large-scale and long-term use is not environmentally sustainable, a fact that could in the future pose limitations toward commercialization. Sn halide perovskites are supposedly less toxic and have a narrower bandgap, which make them better potential candidates for high-performance solar cells. The main problem, however, is their instability as they are prone to self-doping when transforming from Sn^{2+} to Sn^{4+}. To circumvent this challenge, compositional engineering and doping engineering are plausible strategies to employ, having been shown to be viable means of controlling the crystal growth, structural stability, and light conversion properties of most perovskite materials.[20–24] Strontium (Sr) is one of the metal dopants found to exhibit multiple functions such as enhancing device performance and stability of the host perovskite. The ionic radius of Sr is virtually identical to the one of Sn (Sr^{2+}: 1.18 Å and Sn^{2+}: 1.18 Å) and has only the 2+ oxidation state, giving rise to the possibility of doping the crystal structure of Sn-based perovskites to stabilize and tune their optoelectronic properties. Furthermore, Sr is highly abundant and environmentally friendly. Although pure Sr halide perovskite is reported to have a very wide bandgap (e.g., 3.6 eV for $MASrI_3$),[25] the observation of a bandgap bowing in Sn–Pb mixtures suggests that a similar effect might also be present in the Sn–Sr system.[26]

Recently, Sr has been explored as a dopant in Pb perovskites and found to have a direct effect on the optoelectronic properties and performance of the devices as well as the material's structural stability. Pérez-del-Rey *et al.* reported a significant increase in the device fill factor from 78% for the pure perovskite to 85% for 2% Sr^{2+}

doping in methylammonium lead iodide ($MAPbI_3$) perovskite.[23] Shai *et al.* also reported a significant increase in the stability of $MAPbI_{3-x}Cl_x$, which they attributed to suppression of the unsaturated Pb in the presence of Sr dopant.[27] Additionally, doping with Sr^{2+} has been shown to be effective in surface passivation with resultant films that had fewer defects.[24,28] Most recently, metal doping has been extended to Sn perovskites. Dimesso *et al.* reported enhanced thermal stability of $MASnI_3$[29] and $FASnX_3$ (X = I, Br)[30] under a nitrogen environment after doping with earth-alkaline ions (Ca^{2+}, Sr^{2+}, and Mg^{2+}).

However, no work has been reported on the influence of strontium doping on formamidinium-based tin perovskite thin films. In fact, the above-mentioned work reported stability of the perovskite only in powder systems. Hence, here we explore the effect of the strontium insertion on the morphological, structural, and photophysical properties of formamidinium tin iodide perovskite thin films. We show drastic changes in the morphology of the perovskite with the addition of strontium. Crystallographic analysis showed, however, no structural changes with respect to the pure tin perovskite below a concentration of 15%. Finally, photoluminescence (PL) spectroscopy reveals the accumulation of strontium on the surface of the films also for concentrations below 15%.

The perovskite precursors: tin (II) iodide (SnI_2) (99.999%) and strontium iodide (SrI_2) (99.99%), were purchased from Sigma Aldrich, while formamidinium iodide (FAI) was purchased from TCI EUROPE N.V and used as received without further purification. *N,N′*-dimethylformamide (DMF) (99.8%) was acquired from Sigma-Aldrich and dimethyl sulfoxide (DMSO) (99.9%) from Alfa Aesar.

Precursor solution of formamidinium tin iodide ($FASnI_3$) perovskite is obtained by dissolving equimolar amounts of FAI and tin iodide (SnI_2) precursors in a mixed solvent of DMF and DMSO at a volume ratio of 4:1 to form a solution of 0.5M in concentration. To prevent the rapid oxidation of Sn^{2+} to Sn^{4+} in solution, the solution is doped with 10% of tin fluoride (SnF_2). The formamidinium strontium iodide ($FASrI_3$) precursor solution is obtained by dissolving equimolar amounts of FAI and strontium iodide (SrI_2) precursors in gamma-butyrolactone (GBL) to form a solution of 0.5M in concentration. To obtain the alloyed $FASn_{1-x}Sr_xI_3$ solution, we mix stoichiometric amounts of $FASnI_3$ and $FASrI_3$ to form solutions with varying Sr/Sn ratios, representing 0%–50% molar concentration of Sr^{2+} in solution.

The films were fabricated on glass substrates, which were ultrasonically cleaned in detergent solution, deionized water, acetone, and isopropanol, sequentially. After drying them in an oven at 140 °C for about 10 min, they were treated with ultraviolet ozone (UV-O_3) for 20 min and then transferred into a nitrogen-filled glovebox immediately for film deposition. The films were fabricated using a two-step spin program with anti-solvent treatment. The spin program was set at 1000 rpm for 10 s and 4000 rpm for 30 s. The anti-solvent (chlorobenzene) was dropped onto the film at about 5 s prior to the end of the spinning. The films were immediately annealed at 100 °C for 10 min.

The scanning electron microscopy (SEM) images were obtained using the FEI Nova Nano SEM 650 with an accelerating voltage of 2–10 kV for the secondary electron images and ~10 kV for the backscattered electron images. The atomic force microscopy (AFM) images were taken using the Bruker NanoScope V in the ScanAsyst mode.

The X-ray diffraction (XRD) was performed at ambient conditions. The x-ray data were collected using a Bruker D8 Advance diffractometer in the Bragg-Brentano geometry and operating with the Cu Kα radiation source (λ = 1.54 Å) and LynxEye detector.

Absorption measurements were taken using UV-Vis-NIR spectrophotometer (Shimadzu UV-3600). The photoluminescence measurements were performed using the second harmonic (400 nm) of a Ti:sapphire laser (repetition rate, 76 MHz; Mira 900, Coherent) to excite the samples. Unless stated otherwise, the illumination power was decreased to 300 μW cw-equivalent by using a neutral density filter, which amounts to a fluence of approximately 337 nJ/cm^2 on the sample. The excitation beam was spatially limited by an iris and focused with a 150-mm focal length lens. Emitted photons were collected with a lens in the reflection geometry from the sample side. Steady-state spectra were collected using a Hamamatsu electron multiplying charge coupled device (EM-CCD) camera, and time resolved spectra were measured using a streak camera in the synchroscan mode. Samples were kept under a nitrogen atmosphere during the measurement.

Confocal laser scanning microscopy was performed by coupling the aforementioned Ti:sapphire laser into an inverted Nikon Eclipse Ti-E microscope system. A 40× Plan Fluor objective was used for focusing of the excitation beam and collection of the PL signal. PL signals were recorded by using photomultiplier tubes operating with detection ranges of (i) 540 nm–640 nm and (ii) 650 nm long-pass.

The alloyed $FASn_{1-x}Sr_xI_3$ ($0 \le x \le 0.5$) perovskite thin films investigated in this work are deposited from solution on glass substrates. The precursor solution of formamidinium tin iodide ($FASnI_3$) perovskite is obtained by dissolving equimolar amounts of formamidinium iodide (FAI) and tin iodide (SnI_2) precursors in a mixed solvent of *N,N′*-dimethylformamide (DMF) and dimethyl sulfoxide (DMSO) at a volume ratio of 4:1. To prevent the rapid oxidation of Sn^{2+} to Sn^{4+} in solution, the solution is doped with 10% of tin fluoride (SnF_2). The formamidinium strontium iodide ($FASrI_3$) precursor solution is obtained by dissolving equimolar amounts of FAI and strontium iodide (SrI_2) precursors in gamma-butyrolactone (GBL). To obtain the $FASn_{1-x}Sr_xI_3$ solution, we mix stoichiometric amounts of $FASnI_3$ and $FASrI_3$ to form films with varying Sr/Sn ratios, from 0% to 50% molar concentration of Sr^{2+} in solution. The thin films are deposited by spin coating and are annealed at 100 °C for 10 min. Further experimental details are provided under the Methods section in the supplementary material.

Figure 1(a) presents photographs of the $FASn_{1-x}Sr_xI_3$ ($0 \le x \le 0.5$) perovskite thin films showing the effect of the Sr doping on their colors. While the neat tin-based films are dark brown with a lackluster surface, films with 1%–7.5% Sr are dark brown with increased surface reflectivity. Interestingly, as the Sr concentration increases, a noticeable higher surface reflectivity is observed, which indicates an increased uniformity of the films. The film color gradually changes to reddish brown as the Sr concentration is increased further from 7.5% to 50%. The absorption spectra of the fabricated thin films are reported in Fig. 1(b). The absorption band onset of the neat $FASnI_3$ perovskite is clearly observed at 900 nm wavelength, consistent with previous reports.[21] However, upon addition of Sr to the neat $FASnI_3$, we observe a clear blue-shift in the absorption spectra with increasing Sr concentration. Moreover, contrary to what appears to be a

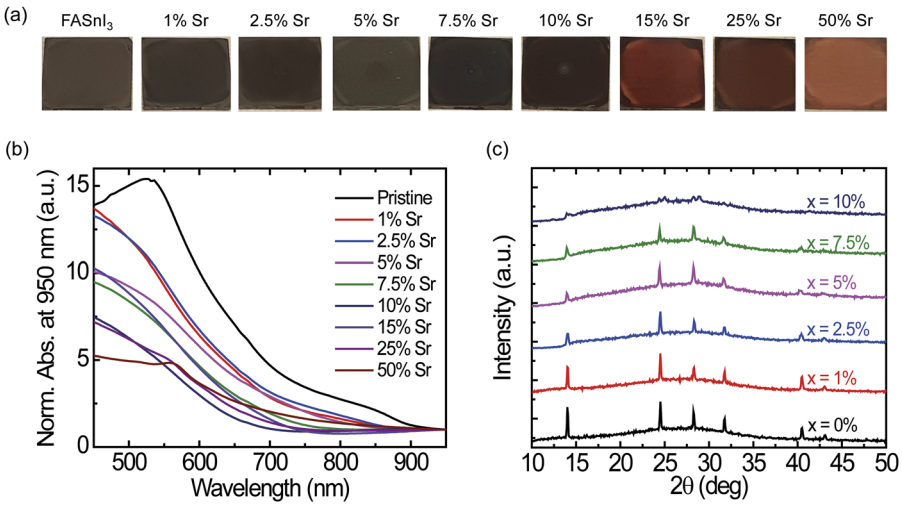

FIG. 1. Photographs and optical and structural characterization of alloyed $FASn_{1-x}Sr_xI_3$ ($0 \le x \le 0.5$) perovskite thin films. (a) Photographs showing $FASnI_3$ thin films with various amounts of Sr doping. (b) UV-Vis absorption spectra normalized at 950 nm, showing the blue-shift of the absorption upon Sr addition and (c) X-ray diffraction patterns of $FASnI_3$ thin films with various Sr%.

strong blue-shift in the absorption peak for the doped samples, the peak intensity rather reduces substantially compared to the neat perovskite film as depicted in the non-normalized absorption spectra shown in Fig. S1 for the 1% Sr sample in comparison with the neat film.

To find the motivation of this band-gap variation, the crystallinity and the structural properties of the films are examined with x-ray diffraction (XRD) measurements. The instability of the films in ambient conditions, which increases with the amount of Sr, made these measurements extremely challenging allowing measurement of only samples with concentrations of Sr between 0% and 10%. As shown in the XRD patterns in Fig. 1(c), the Bragg peaks for both the neat and the strontium-containing films are observed at 2θ values of 14.09°, 24.51°, 28.32°, 31.77°, 40.50°, and 43.11°. Therefore, the addition of Sr has no significant effect on the structural phase of the material at these concentrations. Analysis of the peaks at 14.09° shows that the full-width at half-maximum broadens with increasing the Sr content, which indicates a decrease in the crystal grain sizes. The diffraction intensities of the peaks are also reduced as the Sr content is increased, which could be due to either the low crystallinity of the films with higher Sr concentration or the reduction in crystallinity due to degradation. The decrease in the diffraction peak intensities determined by degradation has been reported for Sr-doped $CsPbI_2Br$ perovskites.[24]

The morphological control of hybrid perovskite thin films is one of the challenges of hybrid perovskite optoelectronics. Scanning electron microscopy (SEM) and atomic force microscopy (AFM) micrographs of the different samples are shown in Fig. 2 and Fig. S1,

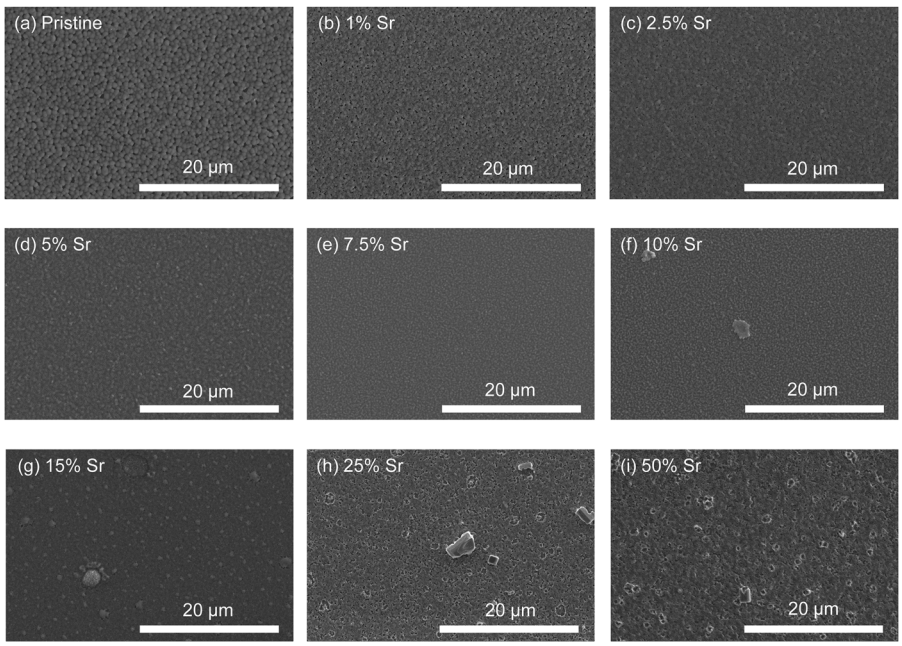

FIG. 2. Thin film morphological characterization. [(a)–(i)] Top-view SEM images of the alloyed $FASn_{1-x}Sr_xI_3$ ($0 \le x \le 0.5$) perovskite thin films showing the films' morphological characteristics for 0%–50% Sr doping.

respectively. Figure 2(a) shows the morphology of the neat $FASnI_3$ perovskite film, which is composed of closely packed crystals with sizes in the 0.5–1 μm range and is characterized by a large number of pores of several hundreds of nanometers width, as well as sharp grain boundaries. The morphology of this reference film is similar to the one previously reported by Shao *et al.*, who showed that such a morphology is a contributing limiting factor to the low efficiency of Sn-based perovskite solar cells.[21] The addition of Sr to the neat perovskite, however, transforms the morphologies substantially. Extreme differences in the film morphologies can be observed, depending on the amount of the Sr^{2+} introduced in the films. The addition of 1%–2.5% of Sr to the neat perovskite, for instance, leads to fused, flatter, and more homogeneous thin films, with grain sizes in the 50–200 nm range and fewer pinholes [Figs. 2(b) and 2(c)]. The films with 5% and 7.5% Sr content also exhibit a unique morphology that varies slightly for the films with 10% and 15% Sr, as shown in Figs. 2(d)–2(g). These films are formed by much smaller grain sizes that are densely packed. As clearly shown in the AFM images (Fig. S2), the films with 10% Sr are highly uniform with completely smeared out grains, with the exception of the appearance of crystallites in the surface. However, as the Sr content is further increased to and above 25%, crystallites appear and the homogeneous and fused domains begin to shrink, leading to the formation of non-continuous films [Figs. 2(h) and 2(i)]. Thus, in general, increasing the Sr content first decreases the crystal grain sizes and then drastically changes the film morphology. The measurement of the film roughness from the AFM images in Fig. S2 shows a decrease in the root-mean-square (rms) roughness from ~50 to ~30 nm going from 0% to 10% Sr. An interesting observation is the formation of large crystallites on the surface of the films for Sr concentrations above 7.5%. As will be validated in the following, our speculation is that these crystallites are composed mainly of Sr-dominated perovskites.

Figure 3(a) shows a photoluminescence intensity map of the neat $FASnI_3$ film obtained using confocal laser scanning microscopy as detected by using a photomultiplier with a 650 nm long pass filter in front (red channel). Likewise, Figs. 3(b) and 3(c) show the spatial distribution of the PL for the 15% and 50% Sr films. Congruent with the SEM micrographs, the neat film shows a relatively uniform PL distribution interrupted by a high density of micrometer-sized pinholes. Upon increasing the Sr content to 15%, the PL distribution becomes less homogeneous and bright features appear throughout the film. The size and distribution of these bright features closely match the features observed in the SEM images of the same film, indicating that the increased PL originates from these surface structures. Increasing the Sr content even further to 50% leads to the formation of larger clusters as well as singular bright spots of various sizes and intensities. For both the neat and 15% Sr films, no PL is detected in the wavelength range from 540 nm to 640 nm [Figs. 3(d) and 3(e)] (green channel). In the case of the 50% Sr film, however, significant PL intensity is recorded in this high-energy channel [Fig. 3(f)]. A comparison of the red and green channels reveals that for the 50% Sr film, we can identify two different types of features in the PL maps; some of the large features that appear brightened in the red channel appear to be dimmer in the green, while some of the smaller spots are relatively bright in both channels. This difference in the local emission spectra corroborates the notion that the film's surface exhibits structures that are compositionally different from the surrounding or underlying perovskite material.

In Fig. 4, we report on the photoluminescence spectra of the thin films upon increasing the strontium content. As displayed in the semi-logarithmic plot in Fig. 4(a), the maximum PL intensity decreases by three orders of magnitude when going from 0% to 50% Sr content. Simultaneously, the emission maximum shifts toward higher energy and thus follows the trend of the bandgaps of the two neat materials ($FASnI_3$ at 1.37 eV and a calculated E_{gap} of 3.6 eV for $MASrI_3$).[21,25] Importantly, this contrasts with the behavior of mixed Sn and Pb perovskites, where the bandgap is narrower for the mixtures than for neat $FASnI_3$.[26] Besides this peak shift, the normalized

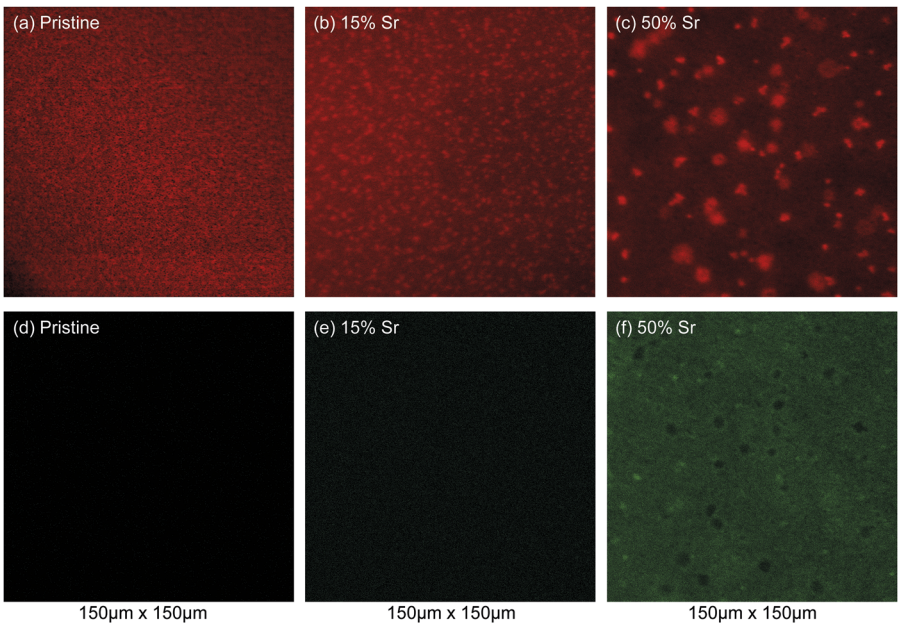

FIG. 3. Confocal laser scanning micrographs of the PL from (a) pristine, (b) 15% and (c) 50% strontium-containing $FASnI_3$ films as detected by a 650 long pass detection channel. [(d)–(f)] PL maps of the same films recorded with a detection channel operating in the wavelength range of 540 nm–640 nm.

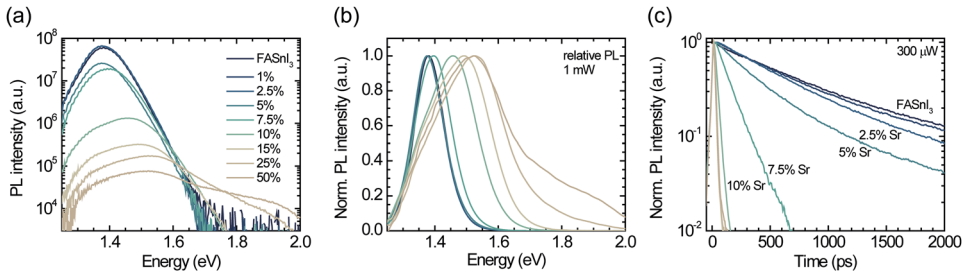

FIG. 4. Photoluminescence (PL) characteristics of Sr-doped $FASnI_3$ perovskite thin films. (a) Non-normalized and (b) normalized steady-state PL emission spectra of $FASnI_3$ perovskite thin films with 0%–50% Sr content. (c) Corresponding time-resolved PL decay of $FASnI_3$ perovskite thin films with 0%–50% Sr content.

spectra in Fig. 4(b) also show a broadening of the emission band. This broadening is mostly due to the appearance of a shoulder in the emission spectra at around 1.38 eV—the energy of the $FASnI_3$ emission peak—whilst the main emission shifts to higher energy for the increased Sr-content. As we shall discuss further below, we attribute this feature to the presence of two different phases in the film.

The transient PL in Fig. 4(c) (taken at the emission maximum) shows a significant PL lifetime reduction already for the smallest additions of Sr to $FASnI_3$. The extracted lifetime amounts to approximately 700 ps for neat $FASnI_3$ and decreases to the instrumental resolution-limited 12 ps for Sr contents exceeding 10% (see Table S1). This behavior is in line with the drastic reduction in PL intensity and underlines the poor quality of these Sr-Sn mixtures.

In all cases, the PL shifts toward higher energy upon increasing the excitation power [Fig. 5(a)]. This effect was previously addressed for neat $FASnI_3$ and attributed to a combination of state filling and emission due to hot charge carriers.[31] Exposure to laser intensities exceeding 20 mW, furthermore, leads to the macroscopic ablation of surface material, as indicated by the black spectrum in Fig. 5(a). The PL from the "bulk" of the thin film is significantly red-shifted (peaking at 1.38 eV for 15% Sr) and much narrower than when compared to the original surface-related PL. A close look also shows that the above-mentioned shoulder around 1.38 eV in the PL spectra is consequently due to this "bulk"-related emission. We thus conclude that our samples possess distinctly different compositions in the "bulk" and at the surface. The blue-shifted PL, furthermore, suggests that Sr is predominantly located at the surface, whilst the emission from the "bulk" is virtually identical to the one of neat $FASnI_3$ or of films with Sr contents below 10%. Crucially, increasing the Sr content beyond 10% also leads to a blue-shift of the bulk-related PL, which shows that Sr is at this concentrations also incorporated into the "bulk" of the film [Fig. 5(b)]. As additional evidence, the streak camera images presented in Fig. S3 also exemplify this effect.

Besides the spectral shift, the bulk-related PL also shows a much longer lifetime than the emission from the surface. Exemplarily, we show the corresponding data for the 7.5% Sr sample in Fig. 5(c). Whilst the emission decays relatively fast on the surface (τ = 128 ps) and becomes even faster for higher excitation intensity, the "bulk" PL shows a much longer lifetime that is close to the one obtained from neat $FASnI_3$ (especially for small Sr concentration).

In summary, we have fabricated $FASn_{1-x}Sr_xI_3$ perovskite thin films with varying concentrations of Sr^{2+} in the range of 0%–50%. The addition of Sr substantially changes the morphology of the perovskite films and blue-shifts the absorption spectra with increasing the Sr content. XRD analysis of 1%-10% Sr-doped perovskite films showed no significant changes to the crystal structure at these concentrations. PL analysis of the doped samples revealed the presence of two distinct phases of the material for Sr contents below 10%: the Sr-deficient bulk and Sr-rich surface phases. However, for Sr contents above 15%, we observed Sr incorporation in the bulk of the material. We therefore conclude that Sr incorporation in these films occurs heterogeneously and predominantly at the surface, while samples of high Sr concentration clearly contain Sr also in the bulk of the sample. This work gives an insight into the properties of alloyed

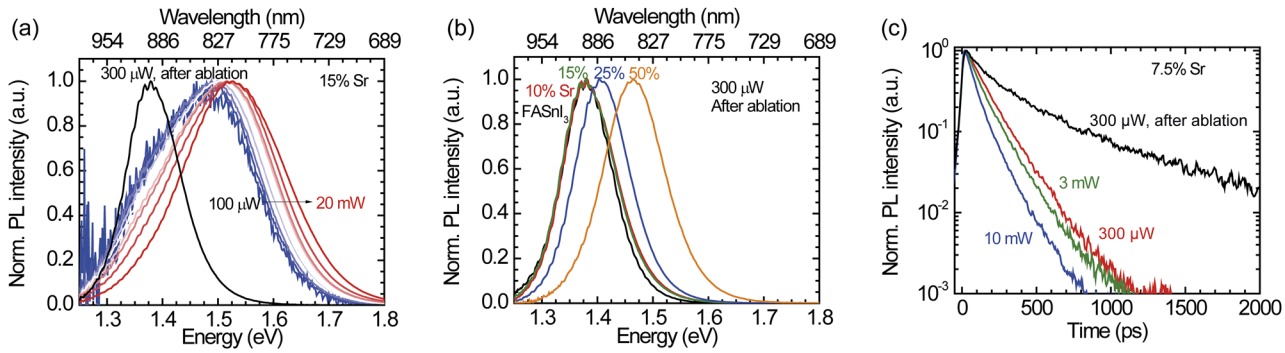

FIG. 5. Excitation power-dependent PL characteristics of Sr-doped $FASnI_3$ thin films. (a) Normalized power-dependent PL spectra of the $FASnI_3$ thin film with excitation power increased from 100 μW to 20 mW for the 15% Sr-doped sample (112 nJ/cm^2-22.5 mJ/cm^2). (b) Normalized PL spectra of $FASnI_3$ perovskite thin films with 0%–50% Sr content obtained after surface ablation of the film. (c) Power-dependent time-resolved PL decay of $FASnI_3$ thin film pumped with different laser intensities for the 7.5% Sr-doped sample.

$FASn_{1-x}Sr_xI_3$ perovskites showing both, interesting properties but also the large potential of Sr-doping in tin perovskites.

See supplementary material for the absorption spectra of the neat and 1% Sr doped samples, AFM images of the 0–10% Sr doped samples, summarized decay lifetime of the 7.5% Sr-doped film, and streak camera images of the 15% Sr containing sample.

We would like to acknowledge the technical support provided by Arjen Kamp and Teodor Zaharia and the experimental assistance by Sameer Rodrigues for the fabrication of the preliminary test samples. This work was funded through the Materials for Sustainability (Mat4Sus) programme by the Netherlands Organisation for Scientific Research (NWO). S. Adjokatse acknowledges financial support from the NWO Graduate Programme, No. 022.005.006, and the Foundation for Fundamental Research on Matter (FOM), which is part of NWO, under the framework of the FOM Focus Group "Next Generation Organic Photovoltaics" for his doctoral studies. S. Kahmann is a research fellow funded through the Deutsche Forschungsgesellschaft (DFG).

REFERENCES

[1] P. Docampo, J. M. Ball, M. Darwich, G. E. Eperon, and H. J. Snaith, Nat. Commun. **4**, 2761 (2013).
[2] C. Roldán-Carmona, O. Malinkiewicz, A. Soriano, G. Mínguez Espallargas, A. Garcia, P. Reinecke, T. Kroyer, M. I. Dar, M. K. Nazeeruddin, and H. J. Bolink, Energy Environ. Sci. **7**, 994 (2014).
[3] X. Hu, X. Zhang, L. Liang, J. Bao, S. Li, W. Yang, and Y. Xie, Adv. Funct. Mater. **24**, 7373 (2014).
[4] A. Kojima, K. Teshima, Y. Shirai, and T. Miyasaka, J. Am. Chem. Soc. **131**, 6050 (2009).
[5] S. Shao, M. Abdu-Aguye, L. Qiu, L.-H. Lai, J. Liu, S. Adjokatse, F. Jahani, M. E. Kamminga, G. H. ten Brink, T. T. M. Palstra, B. J. Kooi, J. C. Hummelen, and M. Antonietta Loi, Energy Environ. Sci. **9**, 2444 (2016).
[6] B. G. H. M. Groeneveld, M. Najafi, B. Steensma, S. Adjokatse, H.-H. Fang, F. Jahani, L. Qiu, G. H. ten Brink, J. C. Hummelen, and M. A. Loi, APL Mater. **5**, 076103 (2017).
[7] Z.-K. Tan, R. S. Moghaddam, M. L. Lai, P. Docampo, R. Higler, F. Deschler, M. Price, A. Sadhanala, L. M. Pazos, D. Credgington, F. Hanusch, T. Bein, H. J. Snaith, and R. H. Friend, Nat. Nanotechnol. **9**, 687 (2014).
[8] X. Dai, Z. Zhang, Y. Jin, Y. Niu, H. Cao, X. Liang, L. Chen, J. Wang, and X. Peng, Nature **515**, 96 (2014).
[9] N. Wang, L. Cheng, R. Ge, S. Zhang, Y. Miao, W. Zou, C. Yi, Y. Sun, Y. Cao, R. Yang, Y. Wei, Q. Guo, Y. Ke, M. Yu, Y. Jin,Y. Liu, Q. Ding, D. Di, L. Yang, G. Xing, H. Tian, C. Jin, F. Gao, R. H. Friend, J. Wang, and W. Huang, Nat. Photonics **10**, 699 (2016).
[10] X. Y. Chin, D. Cortecchia, J. Yin, A. Bruno, and C. Soci, Nat. Commun. **6**(1), 7383 (2015).
[11] F. Maddalena, X. Y. Chin, D. Cortecchia, A. Bruno, and C. Soci, ACS Appl. Mater. Interfaces **10**, 37316 (2018).
[12] S. P. Senanayak, B. Yang, T. H. Thomas, N. Giesbrecht, W. Huang, E. Gann, B. Nair, K. Goedel, S. Guha, X. Moya, C. R. McNeill, P. Docampo, A. Sadhanala, R. H. Friend, and H. Sirringhaus, Sci. Adv. **3**, e1601935 (2017).
[13] F. Deschler, M. Price, S. Pathak, L. E. Klintberg, D. D. Jarausch, R. Higler, S. Hüttner, T. Leijtens, S. D. Stranks, H. J. Snaith, M. Atatüre, R. T. Phillips, and R. H. Friend, J. Phys. Chem. Lett. **5**, 1421 (2014).
[14] H. Zhu, Y. Fu, F. Meng, X. Wu, Z. Gong, Q. Ding, M. V Gustafsson, M. T. Trinh, S. Jin, and X.-Y. Zhu, Nat. Mater. **14**, 636 (2015).
[15] P. Brenner, M. Stulz, D. Kapp, T. Abzieher, U. W. Paetzold, A. Quintilla, I. A. Howard, H. Kalt, and U. Lemmer, Appl. Phys. Lett. **109**, 141106 (2016).
[16] Y. Fang, Q. Dong, Y. Shao, Y. Yuan, and J. Huang, Nat. Photonics **9**, 679 (2015).
[17] L. Dou, Y. M. Yang, J. You, Z. Hong, W.-H. Chang, G. Li, and Y. Yang, Nat. Commun. **5**, 5404 (2014).
[18] S. Yakunin, M. Sytnyk, D. Kriegner, S. Shrestha, M. Richter, G. J. Matt, H. Azimi, C. J. Brabec, J. Stangl, M. V Kovalenko, and W. Heiss, Nat. Photonics **9**, 444 (2015).
[19] H. Wei, Y. Fang, P. Mulligan, W. Chuirazzi, H.-H. Fang, C. Wang, B. R. Ecker, Y. Gao, M. A. Loi, L. Cao, and J. Huang, Nat. Photonics **10**, 333 (2016).
[20] Y. Zhou, J. Chen, O. M. Bakr, and H.-T. Sun, Chem. Mater. **30**, 6589 (2018).
[21] S. Shao, J. Liu, G. Portale, H.-H. Fang, G. R. Blake, G. H. ten Brink, L. J. A. Koster, and M. A. Loi, Adv. Energy Mater. **8**, 1702019 (2018).
[22] M.-C. Wu, W.-C. Chen, S.-H. Chan, and W.-F. Su, Appl. Surf. Sci. **429**, 9 (2018).
[23] D. Pérez-del-Rey, D. Forgács, E. M. Hutter, T. J. Savenije, D. Nordlund, P. Schulz, J. J. Berry, M. Sessolo, and H. J. Bolink, Adv. Mater. **28**, 9839 (2016).
[24] C. F. J. Lau, M. Zhang, X. Deng, J. Zheng, J. Bing, Q. Ma, J. Kim, L. Hu, M. A. Green, S. Huang, and A. Ho-Baillie, ACS Energy Lett. **2**, 2319 (2017).
[25] T. J. Jacobsson, M. Pazoki, A. Hagfeldt, and T. Edvinsson, J. Phys. Chem. C **119**, 25673 (2015).
[26] F. Hao, C. C. Stoumpos, R. P. H. Chang, and M. G. Kanatzidis, J. Am. Chem. Soc. **136**, 8094 (2014).
[27] X. Shai, L. Zuo, P. Sun, P. Liao, W. Huang, E.-P. Yao, H. Li, S. Liu, Y. Shen, Y. Yang, and M. Wang, Nano Energy **36**, 213 (2017).
[28] H. Zhang, H. Wang, S. T. Williams, D. Xiong, W. Zhang, C.-C. Chueh, W. Chen, and A. K.-Y. Jen, Adv. Mater. **29**, 1606608 (2017).
[29] L. Dimesso, C. Das, T. Mayer, and W. Jaegermann, J. Mater. Sci. **53**, 356 (2018).
[30] L. Dimesso, J. Mater. Res. **33**, 4144 (2018).
[31] H.-H. Fang, S. Adjokatse, S. Shao, J. Even, and M. A. Loi, Nat. Commun. **9**, 243 (2018).